ADVANCED HEALTHCARE MATERIALS
www.advhealthmat.de

Mind the Viscous Modulus: The Mechanotransductive Response to the Viscous Nature of Isoelastic Matrices Regulates Stem Cell Chondrogenesis

*Matthew Walker, Eonan William Pringle, Giuseppe Ciccone, Lluís Oliver-Cervelló, Manlio Tassieri, Delphine Gourdon, and Marco Cantini**

The design of hydrogels as mimetics of tissues' matrices typically disregards the viscous nature of native tissues and focuses only on their elastic properties. In the case of stem cell chondrogenesis, this has led to contradictory results, likely due to unreported changes in the matrices' viscous modulus. Here, by employing isoelastic matrices with Young's modulus of ≈12 kPa, variations in viscous properties alone (i.e., loss tangent between 0.1 and 0.25) are demonstrated to be sufficient to drive efficient growth factor-free chondrogenesis of human mesenchymal stem cells, both in 2D and 3D cultures. The increase of the viscous component of RGD-functionalized polyacrylamide or polyethylene glycol maleimide hydrogels promotes a phenotype with reduced adhesion, alters mechanosensitive signaling, and boosts cell–cell contacts. In turn, this upregulates the chondrogenic transcription factor SOX9 and supports neocartilage formation, demonstrating that the mechanotransductive response to the viscous nature of the matrix can be harnessed to direct cell fate.

1. Introduction

The properties of tissue-mimetic hydrogels, including mechanical and biochemical cues, regulate cell adhesion and matrix secretion.[1] In several recent studies, these properties have been tuned for the engineering of articular cartilage tissue, by harnessing the chondrogenic potential of mesenchymal stem cells (MSCs).[2] However, most works disregard the dynamic and dissipative nature of native extracellular matrices (ECMs) and account only for their elastic character. Biological tissues are instead viscoelastic, exhibiting time-dependent stress relaxation in response to an applied strain.[3] Cells are highly sensitive to the factors governing these stress relaxation processes. Indeed, it has been demonstrated that the viscoelasticity of the substrate influences stem cell differentiation and holds a great unexplored potential in controlling stem cell chondrogenesis for cartilage engineering.[4,5] Only a few studies have addressed the effect of hydrogels' viscous behavior on stem cell chondrogenesis, and, in those cases, the viscous contribution of the materials was accompanied by a variation in their elastic properties or by the confounding effect of exogenous growth factors.[2,6–8] While these reports indicate that the viscous component plays a role in chondrogenesis, uncoupling the viscous contribution from other mechanical or biochemical effects is still missing in literature, and it is of crucial importance for furthering our understanding of how this role unfolds. Gong et al. suggested that the viscous character of the substrate influences cell response depending on the value of the elastic modulus of the material.[9] In the case of compliant (low rigidity) materials, faster stress relaxation processes are thought to increase cell spreading, focal adhesion (FA) formation, and nuclear yes-associated protein 1 (YAP) translocation to the nucleus,[10] compared to slow-relaxing ones. Instead, in stiff (high rigidity) environments, fast-relaxing materials are correlated with a rapid viscous dissipation of cell-generated traction forces, reducing spreading and actin stress fibers' organization compared to slow-relaxing counterparts.[11] Moreover, the viscous character of hydrogels has also been associated with chondrogenesis when mature chondrocytes are used for cartilage engineering instead of MSCs. Indeed, faster relaxing gels promoted secretion of an interconnected cartilage matrix by bovine articular chondrocytes; slower relaxing gels, instead, restricted this chondroinductive process.[12]

MSCs are a well-established cell source for cartilage engineering as an alternative to chondrocytes. While the latter are

M. Walker, E. W. Pringle, G. Ciccone, L. Oliver-Cervelló, D. Gourdon, M. Cantini
Centre for the Cellular Microenvironment
University of Glasgow
Glasgow G128QQ, UK
E-mail: marco.cantini@glasgow.ac.uk

M. Walker, E. W. Pringle, G. Ciccone, L. Oliver-Cervelló, M. Tassieri, D. Gourdon, M. Cantini
Division of Biomedical Engineering, James Watt School of Engineering
University of Glasgow
Glasgow G128QQ, UK

The ORCID identification number(s) for the author(s) of this article can be found under https://doi.org/10.1002/adhm.202302571

DOI: 10.1002/adhm.202302571

employed in current clinical approaches to repair cartilage defects, such as autologous chondrocyte implantation,[13] their use is hindered by difficulties in cell sourcing, limited proliferative capacity, and possible formation of fibrocartilage.[14] On the other hand, MSCs are readily expandable in culture, can be isolated from various tissue sources, and have great potential in cartilage tissue engineering via their differentiation into chondrocytes.[15] Indeed, MSCs are highly sensitive to the properties of their environment through integrin-mediated interactions with adhesive motifs such as arginyl-glycyl-aspartic acid (RGD). Hence, hydrogels with optimized biomechanical and biochemical cues can direct MSC differentiation toward particular lineages.[16] In terms of chondrogenesis, it has been suggested that cell spreading and strong FA attachments are not necessary or beneficial, with a low tension rounded stem cell morphology being more chondroinductive.[17] An aggregated and clustered phenotype, typical of the mesenchymal condensation that occurs during cartilage development in embryogenesis, is also known to promote chondrogenesis of MSCs. This can be facilitated in vitro by encouraging cell–cell interactions in a highly dense 3D cellular environment,[18] targeting key chondrogenic signaling events associated with *N*-cadherin and β-catenin.[19,20]

Based on these considerations, we have developed a set of viscoelastic hydrogel matrices that support a chondrogenic phenotype for MSCs via targeting of mechanosensitive pathways. More specifically, we have designed RGD-functionalized matrices for 2D and 3D studies using polyacrylamide (PAAm) and polyethylene glycol maleimide (PEG-MAL) hydrogels with isoelastic moduli of ≈12 kPa and variable viscous component (here reported in terms of loss tangent "tan(δ)" varying between 0.1 and 0.25). Collectively, our results indicate that in environments with a high tan(δ), MSCs had a rounded phenotype with fewer FAs, lower traction forces, decreased expression of integrin β_1 and β_3, and hindered YAP nuclear translocation compared to an elastic (low tan(δ)) matrix. High instances of MSC clustering were also evident when tan(δ) was higher, correlating with increased *N*-cadherin and decreased β-catenin expression. Ultimately, early and late chondrogenesis were promoted at higher tan(δ) through increased expression of SOX9, collagen type II, and aggrecan, and decreased expression of Runx2, fibrocartilage, and chondrocyte hypertrophy markers. We believe that MSC chondrogenesis can be harnessed simply by controlling the hydrogels' viscous component, providing an environment that facilitates a neocartilage phenotype through regulation of cell adhesion, mechanotransduction, and cell–cell communication.

2. Experimental Section

2.1. Peptides

The names and sequences of peptides that were utilized in the study are provided in **Table 1**.

2.2. Antibodies (Abs)

The names of primary antibodies used in the study, along with their corresponding suppliers, are documented in **Table 2**. Additionally, **Table 3** provides information on the names of secondary antibodies and fluorophore-conjugated phalloidins, accompanied by their respective suppliers.

Table 1. Names and sequences of peptides used (provided by GenScript).

Peptide name	Sequence
RGD	GRGDSPC
FITC-RGD	GRGDSPC plus N-T:FITC-Ahx (N-Terminal)
VPM	GCRDVPMSMRGGDRCG
Scram VPM	GCRDVSPMGRMGDRCG

2.3. Primers

Table 4 provides a list of forward and reverse primers utilized for specific genes in the study.

2.4. Cell Culture Reagents

Table 5 shows the cell culture reagents employed in the study for both basal and chondrogenic cultures of hMSCs.

2.5. Glass Preparation for 2D Studies

12 mm glass coverslips and cover glass slides were RCA cleaned by washing in water and ethanol before heating for 10 min at 65 °C in a 5:1:1 solution of water:H_2O_2:NH_3. After drying, cover glass slides were covered with Rain-X for 5 s, washed in ethanol, and dried to use as hydrophobic glass slides. RCA-cleaned 12 mm coverslips were treated with specific silanes for either PAAm or PEG-MAL hydrogel fabrication in 2D. For PAAm hydrogels, coverslips were acryl-silanized by submerging for 2 h in a 0.5% solution of 3-(acryloyloxy)propyltrimethoxysilane (Alfa Aesar) in ethanol with 5% water. Coverslips were then dried and tempered by incubating for 1 h at 120 °C. For PEG-MAL hydrogels, coverslips were thiol-silanized by submerging for 3 h in a 10% solution of (3-Mercaptopropyl)trimethoxysilane (Sigma Aldrich) in toluene before tempering by incubating at 100 °C for 1 h.

Table 2. Names of primary Abs and suppliers used.

Abs	Supplier	Product code	Dilution
SOX9	Santa Cruz	sc-166505	1:250
Lamin B1	ProteinTech Group	66095-1	1:250
Lamin A/C	Santa Cruz	sc-376248	1:250
Aggrecan	Santa Cruz	sc-67513	1:250
COL2A1	Santa Cruz	sc-518017	1:250
COL1A1	Santa Cruz	sc-59772	1:250
COL10A1	Abcam	ab58632	1:200
YAP	Santa Cruz	sc-101199	1:250
Runx2	Santa Cruz	sc-390351	1:250
N-cadherin	BD Biosciences	610920	1:250
p-FAK	Millipore	05-1140	1:250
Piezo1	Novus Bio	NBP1-78537	1:50

Table 3. Names of secondary Abs and fluorophore-conjugated phalloidins used with their suppliers.

Abs	Supplier	Product code	Dilution
Alexa Flour 488	Thermo Fisher	A-11055/A-11008	1:250
Alexa Flour 488 phalloidin	Thermo Fisher	A12379	1:250
Alexa Flour 647 phalloidin	Thermo Fisher	A30107	1:250
Cy3-conjugated	Jackson ImmunoResearch	111-165-003/715-165-150	1:300

Table 4. List of forward and reverse primers used for specific genes (provided by Thermo Fisher).

Gene	Fwd sequence	Rev sequence
GAPDH	AGGTCGGTGTGAACGGATT	TGTAGACCATGTAGTTGAGG
SOX9	GACTTCCGCGACGTGGAC	GTTGGGCGGCAGGTACTG
COL2A1	CGCAATAGCAGGTTCACGTACA	CGATAACAGTCTTGCCCCACTT
Aggrecan	TCGAGGACAGCGAGGCC	TCGAGGGTGTAGCGTGTAGAGA
COL1A1	TCTGCGACAACGGCAAGGTG	GACGCCGGTGGTTTCTTGGT
COL10A1	CAAGGCACCATCTCCAGGAA	AAAGGGTATTTGTGGCAGCATATT
N-cadherin	CGAGCCGCCTGCGCTGCCAC	CGCTGCTCTCCGCTCCCCGC
β-catenin	TGGATGGGCTGCCTCCAGGTGAC	ACCAGCCCACCCCTCGAGCCC
Integrin β_1	GTGCAATGAAGGGCGTGTT	GTTGCACTCACACACACGACA
Integrin β_3	ACACTGGCAAGGATGCAGTGAATTGTAC	CGTGATATTGGTGAAGGTAGACGTGGC
Piezo1	TCGCTGGTCTACCTGCTCTT	GGCCTGTGTGACCTTGGA

2.6. 2D Hydrogel Fabrication

For PAAm hydrogels, all reagents were acquired from Sigma Aldrich. Briefly, 1 mL volumes were prepared using stock solutions of 40% acrylamide and 2% *N,N'*-methylenebisacrylamide mixed in different ratios for specific gel compositions (**Table 6**). Solution volumes were then made up to 1 mL with milli-Q water, 2.5 µL tetramethylethylenediamine (TEMED), and 7.5 µL 10% ammonium persulfate (APS) and mixed thoroughly. 10 µL of solution was spotted onto hydrophobic glass slides before placing acrylsilanized glass coverslips onto the spots. Gelation was allowed to occur at room temperature for 30 min before detaching and swelling in water overnight at 4 °C.

For PEG-MAL hydrogels, stock solutions of 20 kDa and 40 kDa 8-armed PEG-MAL (Creative PEGWorks), VPM, and RGD peptides were prepared in phosphate buffered saline (PBS). Initially, appropriate amounts of PEG-MAL were mixed together with 2 mM RGD peptide for 1 h at room temperature before adding VPM (calculated to stoichiometrically crosslink all remaining reactive groups of each hydrogel) and PBS to make up to 50 µL and mixing thoroughly (**Table 7**). 10 µL of solution was spotted onto hydrophobic glass slides before placing thiolsilanized glass coverslips onto the spots. Gelation was allowed to occur for 1 h at 37 °C before detaching and swelling in PBS overnight at 4 °C.

Table 5. List of cell culture reagents used for basal and chondrogenic cultures of hMSCs.

Reagent	Supplier/product
Dulbecco's modified Eagle medium (DMEM)	Sigma Aldrich
MSC growth medium 2	Promocell
Fetal Bovine Serum (FBS)	Gibco
GlutaMAX (100×)	Gibco
Sodium pyruvate (100 mM)	Sigma Aldrich
MEM non-essential amino acids (100×)	Gibco
Penicillin/streptomycin (10 000 U mL^{-1})	Sigma Aldrich
Amphotericin B (250 ug mL^{-1})	Gibco
Dexamethasone	Sigma Aldrich
Insulin-transferrin-selenium (ITS) (100×)	Gibco
L-ascorbic acid	Sigma Aldrich
L-proline	Sigma Aldrich
TGF-β3	R&D Biosystems/Biotechne

2.7. Water Absorption

Hydrogels were formed, weighed, and immersed in milli-Q water/PBS, for PAAM/PEG-MAL hydrogels respectively, to swell overnight. After 24 h, the solvent was removed, the hydrated samples were weighed again and the amount of water absorbed was calculated using Equation (1) as follows.

$$\text{Water sorption}\,(\%) = \frac{mt - m0}{m0} \times 100 \quad (1)$$

Equation (1) presents the swelling calculation for hydrogels; where *mt* is the weight of the hydrogel at a certain time and *m0* is the weight of the hydrogel after formation.

2.8. Degradability

PEG-MAL hydrogels were formed, swollen overnight in PBS, and weighed prior to degradation. Then, a protease solution of

Table 6. Acrylamide and *N*,*N*'-methylenebisacrylamide ratios for PAAm hydrogels.

Gel name	Acrylamide vol [µL]	Acrylamide percentage [%]	*N*,*N*'-methylenebisacrylamide vol [µL]	*N*,*N*'-methylenebisacrylamide percentage [%]
PAAm 1	375	15	50	0.1
PAAm 2	687	27.48	25	0.05
PAAm 3	875	35	6.2	0.0124

2.5 mg mL^{-1} collagenase D (Roche) in PBS was prepared and added to cover the samples before incubation at 37 °C. At each timepoint, all supernatant was removed by centrifugation at 4000 × *g* for 5 min and samples were weighed. Fresh protease solution was added at each timepoint and the degradation rate was calculated using Equation (2) as follows.

$$Mloss\,(\%) = \frac{Mi - Mt}{Mi} \times 100 \quad (2)$$

Equation (2) shows the degradability calculation for PEG-MAL hydrogels; where *Mloss* is the percentage of mass lost during degradation, *Mi* is the initial mass after swelling, and *Mt* is the mass at the different timepoints after the addition of the protease solution.

2.9. Peptide Functionalization of PAAm Hydrogels

PAAm gels prepared on coverslips were transferred to multiwell plates before covering with 0.2 mg mL^{-1} sulfosuccinimidyl 6-(4′-azido-2′-nitrophenylamino)hexanoate (sulfo-SANPAH) (Thermo Fisher) solution. Samples were placed in a 365 nm UV light source at a distance of ≈3 inches and exposed for 10 min; this process was repeated three times. Gels were then washed with 50 mM HEPES buffer (pH 8.5) three times before covering with 2 mM RGD peptide solution (prepared in same HEPES buffer) and overnight incubation at 37 °C. Gels were then washed with sterile-filtered milli-Q water to remove excess peptide.

2.10. Atomic Force Microscopy

Using a NanoWizard 3 Bioscience AFM (JPK, Berlin, Germany), all measurements and cantilever calibrations were conducted at 37 °C in aqueous environments (water/PBS for PAAM/PEG-MAL hydrogels respectively). Hydrogel samples were prepared on glass coverslips and superglued securely to tissue culture dishes before covering with liquid. Measurements and calibration of cantilever sensitivity against a stiff surface (tissue culture dish) and of spring constant, using the thermal noise method, were done using the JPK SPM software (version 6.1.192).

Force spectroscopy measurements were performed using a constant cantilever approach speed of 2.0 μm^{-1} s. ≈0.3 N m^{-1} cantilevers (TL-CONT from Nanosensors) mounted with a 20 µm diameter spherical silica tip were used. Nanoindentation measurements were done using an indentation depth of ≈1 µm. Microrheology measurements included a pause segment at constant height of 0.5 s after a ≈1 µm indentation, followed by a 0.4 s oscillation/sine segment at a frequency of 10 Hz and amplitude of 10 nm; this was used to derive the viscoelastic response of the samples. From nanoindentation and microrheology measurements, Young's moduli and loss tangent were calculated using the Hertz model and microrheology processing functions of the JPK DP software (version 6.1.192). Force maps were carried out per sample condition to measure multiple points in different regions of the gels.

Quantitative AFM imaging was performed using ≈0.3 N m^{-1} pyramidal, gold-coated cantilevers (PNP-TR-AU cantilevers from NanoWorld). Images were taken using 256 × 256 pixels within 20 × 20 um^2 regions. Scans were performed with a pixel time of 8 ms using a setpoint of 4.5 nN and 2 µm z-length.

2.11. Rheology

Samples were prepared by forming hydrogels in PDMS molds using 250 µL volumes and allowing them to set before transferring to 6 well plates and swelling overnight at 4 °C. For rheological measurements, samples were mounted onto a Physica MCR 301 rheometer (Anton Paar), and the linear viscoelastic region was determined by carrying out an amplitude sweep from 0.1 to 10% strain at 1 rad s^{-1}. Following this, a constant strain of 1% was used to obtain frequency sweeps from 0.5 to 50 rad s^{-1}.

2.12. Stress Relaxation Measurements

Nanoindentation stress relaxation measurements were carried out using a nanoindentation device (Chiaro, Optics11 Life, Amsterdam, Netherlands) mounted on top of an inverted optical microscope (Zeiss Axiovert 200M, Zeiss). Measurements were performed following an adaptation of the protocol described in ref. [51] using a cantilever with stiffness (k) of 0.52 Nm^{-1} holding a spherical tip of radius (R) of 27.5 µm.

Each gel was placed in a petri dish and stabilized with a drop of superglue between the silanized glass coverslip and the petri

Table 7. PEG-MAL and VPM peptide ratios for PEG hydrogels.

Gel name	PEG-MAL conc. [mg mL^{-1}]	PEG-MAL percentage [%]	VPM conc. [mg mL^{-1}]	VPM percentage [%]
PEG 1	213.5 (20 kDa)	21.35	72.6	7.26
PEG 2	427 (40 kDa)	42.7	72.6	7.26

dish. All measurements were carried out at room temperature (≈23 °C) in milliQ water to maintain the samples' hydration. For each experimental condition, at least 100 indentations were performed, each spaced at least 100 µm from the previous. For each indentation, the probe moved at a strain rate of 5 μms^{-1} until it reached an indentation depth (δ) of 3 µm, which was maintained for 60 s using the instrument's closed feedback Indentation control mode. This differs from most AFMs which maintain a constant height, resulting in an increasing indentation depth over the time of the experiment for viscoelastic materials.[52]

Acquired data was cleaned using a previously published open-source software (available of GitHub, time branch of the project).[51] Briefly, the forward segment of the collected force-displacement (F–z) curves was inspected, and unsuccessful indentations were discarded (i.e., indentations where contact was unsuccessful). Then, all segments were saved in a JSON file for further analysis. To analyze the stress relaxation behavior of the material, a jupyter notebook was developed (https://github.com/GiuseppeCiccone96/stressrelaxnano). Briefly, force-time $F(t)$ curves were first aligned to zero force if their baseline was negative. Then, the maximum of $F(t)$ and its corresponding time was found, yielding the point (t0, F0). Curves were therefore aligned to 0 time by a horizontal shift equal to t0. Following this, the signal was cropped between t0 and the maximum time before retraction, that is, only the part of the signal where the indentation was kept constant was retained. Following this, $F(t)$ was normalized by dividing the whole signal by F0. Because individual curves were too noisy to be analyzed, an average curve was found and used for quantification of the energy dissipation of the materials. Energy dissipation was quantified from the normalized signal using Equation (3) as follows.

$$\text{Energy dissipation}_t = (F_0 - F_t) \times 100 \tag{3}$$

Equation (3) shows the energy dissipation calculation from the normalized stress relaxation signal, where the subscript t denotes the maximum time in the averaged data.

2.13. Mesh Size

The mesh size ξ of the PEG-MAL hydrogels was calculated according to mechanical measurements,[53] swelling measurements,[54] or both.[55] The mesh size based on mechanical measurements was obtained from AFM force spectroscopy according to the following Equation (4).[56]

$$\xi = ((GN_A)/RT)^{(-1/3)} \tag{4}$$

Equation (4) defines mesh size based on mechanical testing, where N_A is the Avogadro number, R is the molar gas constant, T is the temperature at which measurements were made and G is the shear modulus obtained from Equation (5).

$$G = \frac{E}{2(1+\nu)} \tag{5}$$

Equation (5) shows the relationship between shear modulus G and Young's modulus E obtained via AFM force spectroscopy, where ν is the Poisson ratio, assumed to be 0.5 (incompressible rubber-like materials).

The mesh size based on swelling measurements was obtained according to Flory-Rehner theory using the following equations from Peppas and Merrill:[57,58]

$$\xi = {\nu_{2,s}}^{-1/3} \left(\bar{r}_0^2\right)^{1/2} \tag{6}$$

Equation (6) shows mesh size ξ as a function of $\nu_{2,s}$, volume fraction of the polymer in the swollen state, and $\left(\bar{r}_0^2\right)^{1/2}$, end-to-end distance of the polymer chain in the unperturbed state, calculated through Equation (7).

$$\left(\bar{r}_0^2\right)^{1/2} = l C_n^{1/2} n^{1/2} \tag{7}$$

In Equation (7), l is the average bond length in the repeating unit of PEG and equal to 0.146 nm,[59] C_n is the characteristic ratio of the polymer (4.0 for PEG),[60] and n is the number of repeating units in the crosslink, calculated based on Equation (8).

$$n = 2\frac{\overline{M_c}}{M_r} \tag{8}$$

In Equation (8), M_r is the molecular mass of the repeating unit of the polymer (44 for PEG)[60,61] and $\overline{M_c}$ is the average molecular weight between crosslinks calculated from swelling behavior according to Equation (9).[57]

$$\frac{1}{\overline{M}_c} = \frac{2}{\overline{M}_n} - \frac{\left(\frac{\bar{v}}{V_1}\left[ln\left(1-\nu_{2,s}\right) + \nu_{2,s} + \chi\nu_{2,s}^2\right]\right)}{\nu_{2,r}\left[\left(\frac{\nu_{2,s}}{\nu_{2,r}}\right)^{1/3} - \frac{1}{2}\left(\frac{\nu_{2,s}}{\nu_{2,r}}\right)\right]} \tag{9}$$

In Equation (9), $\overline{M_n}$ is the number-average molecular weight of the polymer, $\bar{v}$ is the specific PEG volume in amorphous state (0.89 $cm^3\ g^{-1}$), V_1 is the molar volume of water (18 $cm^3\ mol^{-1}$), X is the Flory PEG-water interaction parameter (0.426)[60] and $\nu_{2,r}$ is the polymer volume fraction before swelling.

Finally, mesh size according to mechanical testing and swelling behavior can be calculated based on Equations (6)–(8), where $\overline{M_c}$ was calculated through Equation (10)[62] instead of Equation (9).

$$\frac{1}{\overline{M}_{C,E}} = \frac{GQ^{1/3}}{RTC_{2,r}} + \frac{2}{\overline{M_n}} \tag{10}$$

In Equation (10), $C_{2,r}$ is the mass concentration of the polymer in solution before crosslinking and Q is the water-induced volumetric swelling ratio, calculated according to Equation (11).

$$Q = \frac{\nu_{2,r}}{\nu_{2,s}} \tag{11}$$

Equation (11) shows the water-induced volumetric swelling ratio.

2.14. Cell Culture

Primary human mesenchymal stem cells (hMSCs) (Promocell) were thawed and resuspended in MSC growth medium 2 with supplement mix (Promocell) for expansion. Prior to seeding on or in the hydrogels, cells were serum-starved overnight in DMEM containing 1% FBS. Cells were harvested by trypsinization at 70–80% confluency and cultured in a basal media of DMEM containing 10% FBS with biweekly media changes. High-glucose DMEM was used and supplemented with GlutaMAX (1×), sodium pyruvate (1 mM), non-essential amino acids (1×), penicillin/streptomycin (1%), and amphotericin B (2.5 µg mL^{-1}). Throughout all culturing, cells were incubated at 37 °C in a 5% CO_2 atmosphere.

For chondrogenic media cultures, modified DMEM was used containing 100 nM dexamethasone, 1× ITS, 50 µg mL^{-1} L-ascorbic acid-2-phosphate, 40 µg mL^{-1} L-proline and 10 ng mL^{-1} TGF-ß3.

2.15. 2D Cell Seeding

For 2D cell studies, hydrogels on coverslips were sterilized under UV light for 30 min. Then, trypsinized cells were suspended in an appropriate cell culture medium and seeded onto hydrogels at a density of 5000 cells cm^{-2}.

2.16. 3D Cell Encapsulation in PEG-MAL Hydrogels

For 3D cell studies, all PEG-MAL hydrogel reagents were sterilized under UV light for 30 min. Then, PEG-MAL was allowed to react with RGD peptide for 1 h at room temperature while preparing cell pellets. Cell pellets were prepared by washing trypsinized cells in PBS via centrifugation (200 × *g* for 5 min) to remove any presence of media components. Cell pellets were then suspended in the RGD-functionalized PEG-MAL solution at a density of 4 million cells mL^{-1} before adding VPM peptide and PBS to make up to 50 µL volumes. The full volume was pipetted into a multiwell plate and gelation was allowed to occur in a cell culture incubator for 1 h. The cell-laden gels were then immersed in the appropriate cell culture medium and allowed to recover in the incubator for 1 h before being replaced with fresh media for culturing.

2.17. 3D Sectioning

3D cultures were fixed using 4% formaldehyde for 30 min at 4 °C before exchanging with 30% sucrose in PBS overnight at 4 °C. Samples were then included in optimal cutting temperature compound (OCT) in cryomolds and frozen using liquid nitrogen before storage at −80 °C. Samples were cut using a cryotome in 20 µm sections and frozen at −80 °C prior to immunostaining.

2.18. Immunostaining

2D samples were washed with PBS before fixing with 4% formaldehyde for 30 min at 4 °C. 3D samples were sectioned after fixing as explained above. Then, PBS washes were done followed by permeabilization in 0.1% Triton X-100 for 5 min at room temperature. Samples were then washed with PBS and blocked for 1 h in 1% bovine serum albumin (BSA). After blocking, all primary Ab solutions were prepared in 1% BSA at appropriate dilutions (Table 2) and added to cover the samples before incubating overnight at 4 °C. After primary Ab incubations, samples were washed three times with 0.5% Tween-20 prior to addition of secondary Ab solutions (diluted appropriately in 1% BSA, Table 3) and incubation at room temperature in the dark for 1 h. Samples were then washed three times with 0.5% Tween-20 before mounting onto glass slides using VECTASHEILD antifade mounting medium with DAPI (Vector Laboratories). Visualization was done using a fluorescence microscope (Zeiss AxioObserver Z1).

2.19. Image Analysis

Image processing was done using ImageJ (version 1.53t). Cells were measured by binarising nucleus and/or actin cytoskeleton in images using a threshold function. Then, the wand tracing tool was used to select the outline of the thresholded areas, and the measure function was used to calculate morphological parameters, such as cell area and circularity; protein expression levels were measured via integrated density, normalized to cell number based on count of nuclei. YAP expression was represented as a nuclear/cytoplasmic ratio; this was performed by measuring nuclear and cytoplasmic YAP expression independently and calculated as follows:

$$\mathrm{YAP}_{\mathrm{nuc/cyt}}\ \text{ratio} = \left[\left(\mathrm{YAP}_{\mathrm{nuc}}/A_{\mathrm{nuc}}\right) / \left(\mathrm{YAP}_{\mathrm{cyt}}/A_{\mathrm{cyt}}\right)\right] \quad (12)$$

Equation (12) defines YAP's integrated density fluorescence nucleus/cytoplasm ratio; where $\mathrm{YAP}_{\mathrm{nuc}}$ is the integrated density of YAP in the nucleus, A_{nuc} is the area of the nucleus, $\mathrm{YAP}_{\mathrm{cyt}}$ is the integrated density of YAP in the cytoplasm (Equation (13)), and A_{cyt} is the area of the cell cytoplasm (Equation (14)).

$$\mathrm{YAP}_{\mathrm{cyt}} = \mathrm{YAP}_{\mathrm{cell}} - \mathrm{YAP}_{\mathrm{nuc}} \quad (13)$$

Equation (13) shows YAP's integrated density fluorescence in the cytoplasm; where $\mathrm{YAP}_{\mathrm{cell}}$ is the integrated density of YAP in the entire cell

$$A_{\mathrm{cyt}} = A_{\mathrm{cell}} - A_{\mathrm{nuc}} \quad (14)$$

Equation (14) provides the definition of cytoplasmic area; where A_{cell} is the area of the entire cell.

Focal adhesion analysis was performed on p-FAK stained samples using a previously described step-by-step method[63] and implementing it in ImageJ. Actin fiber anisotropy was performed using the FibrilTool plug-in as previously described.[64]

2.20. Pharmacological Inhibition

Pharmacological inhibition of Rac1 and ROCK activity was achieved using 50 µM NSC-23766 (Tocris Bioscience) and 10 µM Y-27632 (Calibiochem) respectively. Inhibitors were added to cell cultures 1 h prior to fixing.

2.21. Traction Force Microscopy

Carboxylate-modified 0.2 µm FluoSpheres (Life Technologies) were prepared by sonicating the stock for 10 min. This was then diluted 1:30 in milli-Q water and further sonicated for 15 min. Immediately after sonication, 1:25 of bead dilution was incorporated into the gel recipes for PAAm hydrogels on coverslips before functionalization with 2 mM RGD peptide (as previously described). Cells were seeded on the 2D gel surfaces (as described previously) and allowed to adhere for 24 h. Using an EVOS FL Auto microscope (Life Technologies), Z-stack images were taken through the samples before and after trypsinization; stacks were acquired at 1 µm intervals between the highest and lowest position where beads were visible. Using ImageJ software, z-projections of acquired z-stacks were generated and cell traction forces were determined by tracking the displacement of the FluoSpheres and then reconstructing the force field from the displacement data using the iterative particle image velocimetry (PIV) and FTTC plugins respectively,[65] available at https://sites.google.com/site/qingzongtseng/tfm.

An explanation of the computational method is outlined at https://www.theses.fr/2011GRENY027/abes, and is briefly recapitulated below.

Considering that the deformation (displacement) parallel to the gel surface caused by cellular traction was smaller than the thickness of the gel, the gel could be represented as a semi-infinite half space. The displacement $u(x_1,x_2)$ on the surface of this half space is described as the convolution between the point forces $f(x'_1,x'_2)$ and the elastic Green's tensor function $G_{ij}(x_1 - x'_1,x_2 - x'_2)$, where the subscript index ij takes on values from 1–2 assuming that the force and displacement orthogonal to the gel surface is negligible (Equation (15)).

$$u_i(x) = \int \sum_j G_{ij}(x - x') f_j(x')\, dx' \tag{15}$$

Equation (15) elucidates that the solution for the force field requires the deconvolution of the displacement field with Green's function.

$$\tilde{u}_{ik} = \left\{ \sum_j \tilde{G}_{ij} \tilde{f}_j \right\}_k \tag{16}$$

In the Fourier space, Equation (15) can be rewritten to give Equation (16), where subscript k stands for the mode (number of basis function) in the frequency domain; where $\tilde{f}$ is the force field in the Fourier space, $\tilde{u}$ is the displacement field in Fourier space and $\tilde{G}$ is the elastic Green's function in Fourier space as expressed below in Equation (17).

$$\tilde{G}_k = \frac{2(1+\nu)}{Ek^3} \begin{pmatrix} (1-\nu)k^2 + \nu k_y^2 & -\nu k_x k_y \\ -\nu k_x k_y & (1-\nu)k^2 + \nu k_x^2 \end{pmatrix} \tag{17}$$

Equation (17) expresses $\tilde{G}$ as the elastic Green's function in Fourier space where E is the Young's elastic modulus, ν is the Poisson ratio, and k is the corresponding wavevector in Fourier space.

$$\tilde{f}_{ik} = \left\{ \sum_j \tilde{G}_{ij}^{-1} \tilde{u}_j \right\}_k \tag{18}$$

Equation (18) represents the traction vector field in Fourier space, where $\tilde{G}_{ij}^{-1}$ denotes the inversion of the 2D Green's tensor.

$$\tilde{f}_{ik} = \left\{ \sum_{l,j} \left[\sum_m \tilde{G}_{ml} \tilde{G}_{mi} + \lambda^2 I \right]^{-1} \tilde{G}_{jl} \tilde{u}_j \right\}_k \tag{19}$$

Equation (19) finally represents the regularization scheme implemented to Equation (18) to give an efficient and reliable force reconstruction.

2.22. qPCR

All reagents were provided by QIAGEN unless otherwise stated. Cell lysis and RNA extraction were performed using an RNeasy mini kit. For 2D samples, cells were directly lysed on the surface of the gels before RNA extraction. For 3D samples, cells were released by incubating gels in a cell culture incubator in a protease solution of 2.5 mg mL^{-1} collagenase D (Roche) in PBS until gels were fully degraded. Cells were pelleted via centrifugation (200 × *g* for 5 min) and then lysed for RNA extraction using an RNeasy Micro Kit. RNA quantity and purity were measured using a NanoDrop 1000 (Thermo Scientific) before performing cDNA synthesis using a QuantiTect Reverse Transcription kit. Real-time qPCR was performed using a model 7500 real-time PCR machine (Applied Biosciences) using SYBR green reagents from a QuantiFast SYBR Green PCR kit. 4 ng cDNA was used per gene, primers were used at 1 µM concentrations and GAPDH was used throughout as a housekeeping gene for normalization of fold-changes in gene expression.

2.23. Sulfated GAG Quantification

After 3 weeks, 3D cultures were treated with 200 µg mL^{-1} proteinase K solution (Sigma Aldrich) for 18 h at 56 °C. The solution was then mixed with an equal volume of 1,9-dimethylmethylene blue (DMB) solution (45.9 µM DMB, 40.5 mM glycine, 27.3 mM NaCl, pH 3-3.5) immediately before absorbance readings at 525 nm using an Infinite 200 Pro plate reader (Tecan); samples were calibrated against a standard curve of chondroitin sulfate (Sigma Aldrich).

2.24. Cell Viability

Cells were encapsulated in PEG-MAL hydrogels and cultured in basal media. After 24 h, CCK-8 solution (Sigma Aldrich) was prewarmed for 5 min at 37 °C, added into the culture medium at a 10% concentration, and incubated for 4 h in a cell culture incubator. The solution was then removed, transferred to a multiwell

plate, and measured at an absorbance of 450 nm by a NanoQuant Infinite M200 Pro plate reader (Tecan). Fresh media was added to the samples and the process was repeated after a further 24 h of culture.

2.25. Statistical Analysis

Data are represented as mean ± SD and were analyzed using GraphPad Prism software where normality tests (Anderson-Darling, D'Agostino & Pearson, Shapiro-Wilk and Kolmogorov-Smirnov) were performed to determine whether to select parametric or non-parametric tests. Then, appropriate one-way ANOVA or *t*-tests, for multiple or pairwise comparisons respectively, were used and differences were considered significant for $p \leq 0.05$ (* $p \leq 0.05$, ** $p \leq 0.01$, *** $p \leq 0.001$). For *t*-tests: if normality tests were passed, unpaired *t*-tests with Welch's correction were performed; if normality tests failed, Mann-Whitley tests were performed. For one-way ANOVAs: if normality tests were passed, Brown-Forsythe and Welch tests were performed; if normality tests failed, Kruskal-Wallis tests were performed.

3. Results

3.1. Fabrication and Characterization of Isoelastic Hydrogels with Variable Viscous Component

PAAm hydrogels are widely used for 2D cell studies due to their highly tunable mechanical properties and ease of functionalization with ECM peptides, such as RGD, to promote cell adhesion.[21] They can be fabricated with controlled viscoelastic properties using various strategies, such as incorporating linear, high molecular weight PAAm chains.[22] Here, we optimized an alternative strategy to tune PAAm viscoelasticity by fabricating gels with high polymer content and relatively low crosslinking, encouraging physical entanglement of polymer chains (**Figure** 1A), as suggested previously by Cameron et al.[23] PEG-MAL hydrogels are instead suitable for 3D cell studies due to their lack of toxic precursor components, which are present in PAAm hydrogels.[24] The maleimide groups of PEG-MAL are crosslinked and functionalized with thiolated peptides at physiological pH through Michael-type addition, forming bioactive and cytocompatible hydrogels.[25] We used 8-armed PEG-MAL to fabricate hydrogels and controlled their viscoelastic properties by adjusting polymer molecular weight (Figure 1A); this strategy has also been effective with other material systems such as alginate.[26] The specific compositions of each hydrogel can be found in the Experimental Section.

By using atomic force microscopy (AFM), we found that all PAAm and PEG-MAL hydrogels had similar Young's moduli of ≈12 (±1) kPa through nanoindentation measurements. We selected this as an appropriate stiffness based on previous literature using a similar stiffness regime to investigate stem cell mechanosensing and chondrogenesis; in general, the stiffness range typically used for hydrogel-supported chondrogenesis across recent literature is between low kPa up to 10's of kPa.[2,27] Additional microrheology testing of our hydrogels revealed loss tangent values ranging between ≈0.1 and ≈0.25 (Figure 1B). We also observed that the encapsulation of MSCs within PEG-MAL hydrogels did not significantly impact the gels' mechanics (Figure 1B). Bulk rheology measurements confirmed that the hydrogels displayed similar shear elastic moduli and variable viscous moduli, as shown in Figure S1A, Supporting Information. The viscoelastic properties of the hydrogels were further assessed by stress relaxation measurements, which revealed that PAAm and PEG-MAL hydrogels with higher loss tangent values displayed faster stress relaxation (Figure 1C) and higher energy dissipation (Figure S1B, Supporting Information), in agreement with previous studies.[10,12,26] We were also able to control the biodegradability of the PEG-MAL hydrogels by adjusting the ratio of the protease-sensitive peptide GCRDVPMSMRGGDRCG (VPM) relative to a scrambled non-degradable counterpart during crosslinking of the hydrogels (Figure 1D). We observed that adjusting hydrogel degradability did not influence swelling behavior, indicating that the macromolecular structure and porous network of the hydrogels were unaffected (Figure S2A,B, Supporting Information). Moreover, AFM imaging of all hydrogels revealed a similar topography independently of gel composition and mechanical properties, as indicated by similar roughness values among the PAAm hydrogels (Figure S2Ci, Supporting Information) and between the PEG-MAL hydrogels (Figure S2Cii, Supporting Information). Finally, the PEG-MAL hydrogels were also found to have a similar mesh size, calculated based on swelling and mechanical measurements (Figure S2D, Supporting Information).

3.2. The Viscous Character of Isoelastic Matrices Regulates hMSC Adhesion and Spreading

Hydrogels were functionalized with 2 mM RGD peptide to facilitate cell adhesion, as neither PAAm nor PEG-MAL contain naturally occurring cell binding sites. Using fluorescently labeled RGD, we observed uniform ligand densities across the PAAm hydrogels' surfaces, indicating similar availability of cell adhesion sites (Figure S3, Supporting Information). We also verified that cells were viable when encapsulated within the PEG-MAL hydrogels, confirming their suitability for 3D culture (Figure S4, Supporting Information). Given the aim of this paper, and the successful achievement of isoelastic hydrogels, from now on all samples are discriminated by means of their relative loss tangent tan(δ) values; moreover, for PEG-MAL hydrogels, 1% of the degradable crosslinker VPM is used unless stated otherwise.

After seeding human MSCs (hMSCs) on the surface of PAAm hydrogels, we observed striking differences in their spreading behavior and FAs size and number. On substrates with a higher tan(δ) cell spreading was diminished, as demonstrated by reduced cell area and increased circularity (**Figure** 2Ai,ii); this coincided with a reduction in phosphorylated-focal adhesion kinase (p-FAK) intensity, average FA length, and frequency of FAs over 2 µm (Figure 2Aiii). Previous work has shown that a rounded MSC phenotype encourages chondrogenesis in 2D with low, non-localized vinculin expression.[17] We observed the same behavior in cell spreading and circularity for hMSCs on 2D PEG-MAL hydrogels with increased tan(δ) (Figures S5 and S6C, Supporting Information). Analysis of various hMSC cytoskeletal

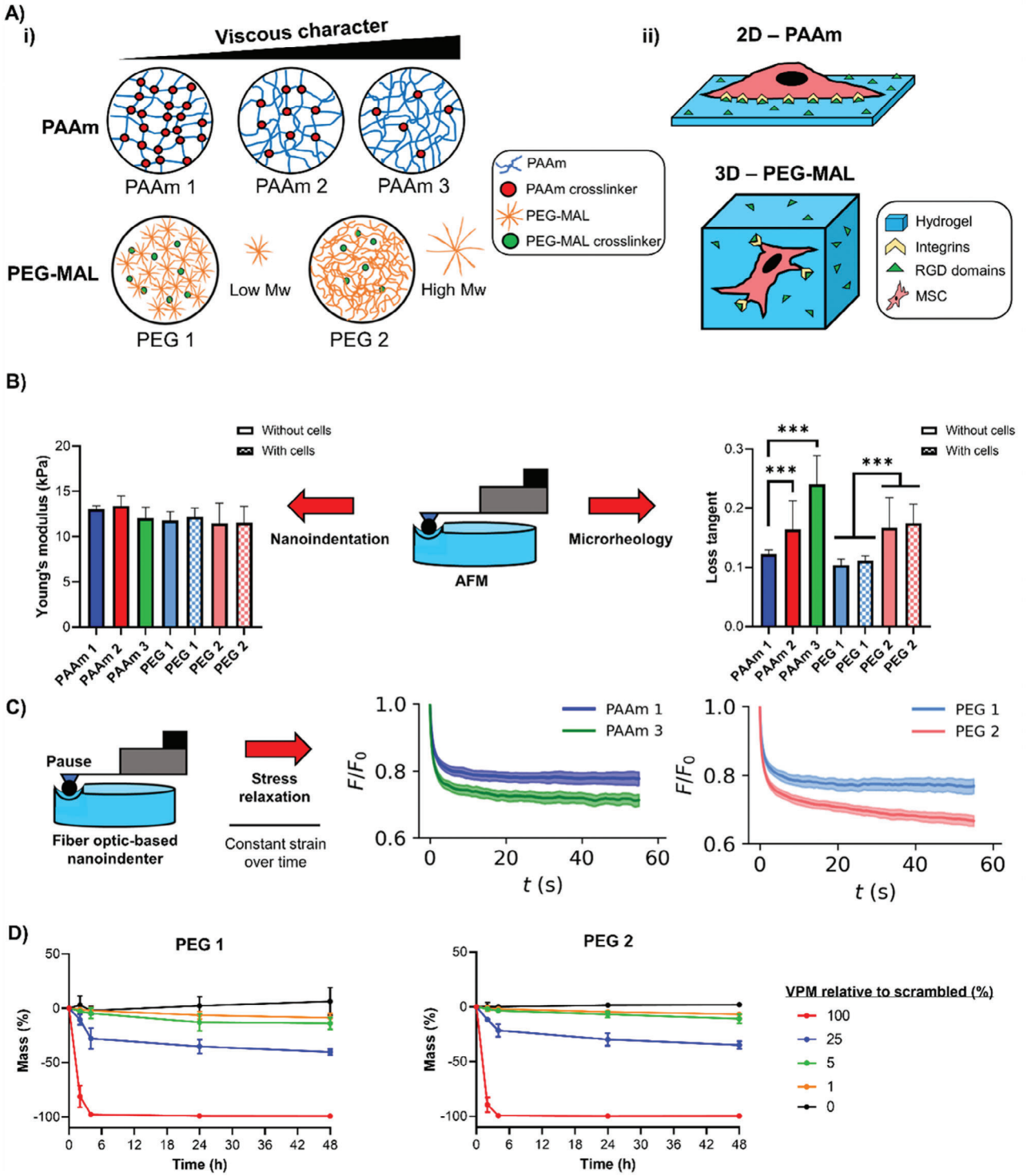

Figure 1. PAAm and PEG-MAL isoelastic hydrogels with tuneable viscous component. A-i) Representation of PAAm and PEG-MAL polymer:crosslinking ratios and molecular weight differences within hydrogels and the influence on their loss tangent and ii) sketch of 2D/3D dimensionality of each hydrogel system as cell culture platforms. B) AFM microscale measurements of PAAm and PEG-MAL (crosslinked with 1% VPM relative to scrambled) hydrogels using nanoindentation for Young's modulus (left) and microrheology for loss tangent (right); PEG-MAL hydrogels were measured without cells and in the presence of encapsulated cells; $n = 50–100$. C) Stress relaxation measurements of hydrogels using a fiber-optic-based nanoindenter with pause step for PAAm (left) and PEG-MAL (crosslinked with 1% VPM relative to scrambled) (right) hydrogels, $n = 100$. D) Biodegradability of PEG-MAL hydrogels crosslinked with different degrees of VPM (relative to scrambled VPM) represented by mass loss over 48 h in the presence of collagenase D for PEG 1 (left) and PEG 2 (right), $n = 3$. For all figures, data are represented as mean ± standard deviation and differences are considered significant for $p \leq 0.05$ using one-way ANOVAs for multiple comparisons (*** $p \leq 0.001$).

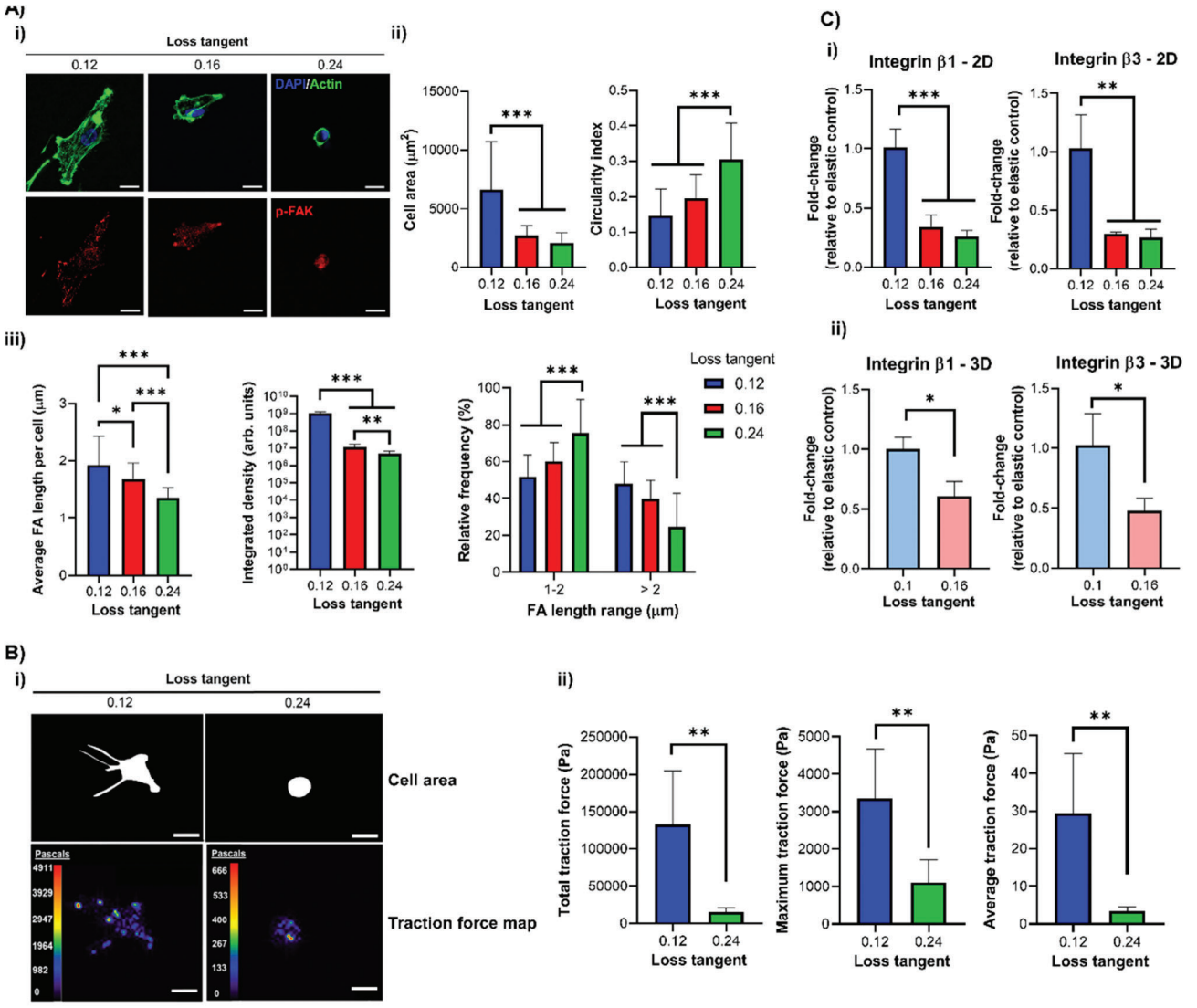

Figure 2. hMSC adhesion and spreading decrease as the matrix viscous component increases. A-i) Representative immunofluorescence images of hMSCs cultured for 24 h on 2D PAAm hydrogels with DAPI (blue), actin (green) and p-FAK (red) staining with ii) quantification of cell area (left) and circularity (right), $n = 31$–35, and iii) quantification of average FA length per cell (left), p-FAK signal intensity (middle) and relative frequencies of FAs between 1–2 μm and >2 μm (right), $n = 25$–50. B-i) Representative images of the cell mask area and traction stress maps with cell traction stresses (in Pascals) for hMSCs cultured for 24 h on 2D PAAm hydrogels and ii) quantification of the total (left), averaged (middle) and maximum (right) traction stresses, $n = 5$. C) qPCR data from hMSCs cultured i) on 2D PAAm and ii) in 3D PEG-MAL gels for 3 days showing fold-change in gene expression of integrin β_1 (left) and β_3 (right) relative to control with stronger elastic character (0.12/0.1 loss tangent samples) and normalized to GAPDH, $n = 3$. For all figures, data are represented as mean ± standard deviation, and differences are considered significant for $p \leq 0.05$ using one-way ANOVA or *t*-tests for multiple or pairwise comparisons respectively (* $p \leq 0.05$, ** $p \leq 0.01$, *** $p \leq 0.001$). All hydrogels were functionalized with 2 mM RGD peptide to allow cell adhesion. All PEG-MAL hydrogels were crosslinked using peptide ratios of 1% VPM and 99% scrambled VPM. Scale bars = 20 μm.

shape descriptors over time showed results consistent with our observations of cell spreading behavior (Figure S6, Supporting Information). These observations agree with previous works using hydrogels with a similar stiffness to ours, where cells were also shown to display reduced spreading as tan(δ) increased.[9–11] It has been suggested that this behavior could be related to rapid energy dissipation of cell-generated traction forces into the matrix, which hinders spreading and activation of mechanoresponsive signaling pathways.[11] Indeed, we observed decreased actin fibers anisotropy for hMSCs on more viscous PAAm gels, implying a reduced cytoskeletal organization of cells on those substrates (Figure S6B, Supporting Information). Correspondingly, hMSCs applied significantly lower traction forces on PAAm hydrogels with a higher loss tangent value than on more elastic ones (Figure 2B). Moreover, the expressions of integrins β_1 and β_3 (known RGD receptors) were significantly reduced for hMSCs interacting with higher tan(δ) hydrogels, indicating less integrin availability for cell attachment via RGD-integrin interactions, both on 2D PAAm hydrogels and within 3D PEG-MAL matrices (Figure 2C).

3.3. hMSC Mechanotransduction Is Regulated by the Viscous Component of Isoelastic Matrices

Next, we investigated whether the viscous component of our matrices also affected mechanotransduction, driving transcriptional control through regulators such as YAP.[4] YAP has been identified in previous work as a negative regulator of chondrogenesis in MSCs;[28] however, the role of mechanosensitive YAP signaling is relatively unexplored in hydrogel-driven chondrogenesis, despite its established role as a mechanical rheostat.[29] Here, we observed decreased nuclear YAP localization on PAAm hydrogels with a higher loss tangent, implying reduced YAP-mediated transcriptional regulation of anti-chondrogenic target genes (**Figure 3**A). We observed the same effect for PEG-MAL hydrogels with a higher tan(δ), both in 2D (Figure S7, Supporting Information) and in 3D (Figure 3B).

ROCK and Ras-related C3 botulinum toxin substrate 1 (Rac1) signaling are important events in the regulation of cytoskeletal organization. Inhibition of ROCK signaling via Y-27632 has been shown to cause increased chondrogenesis;[7,30] this suggests that reduced cytoskeletal tension is beneficial to facilitate a chondrogenic phenotype. Here, we observed that inhibition of ROCK or Rac1 signaling reduced nuclear YAP translocation in hMSCs on PAAm hydrogels with a stronger elastic character; combined ROCK and Rac1 inhibition reduced nuclear YAP further and facilitated a phenotype similar to that of cells on more viscous hydrogels (Figure S8, Supporting Information). On the other hand, inhibition of ROCK and Rac1 signaling had no influence on nuclear YAP in hMSCs seeded on PAAm hydrogels with a higher loss tangent; only the inhibition of both caused a slight reduction in translocation (Figure S8, Supporting Information). Collectively, these results suggest that ROCK and Rac1 signaling are significantly less active in cells on hydrogels with a high tan(δ), indicating a more chondrogenic environment.

Lamins are major structural and mechanotransductive proteins of the nucleus. It has been shown that MSCs on soft matrices exhibit a less spread nucleus and low levels of lamin A/C expression due to its rapid phosphorylation in response to reduced cytoskeletal tension.[31] We observed that on hydrogels with a higher tan(δ), the ratio of lamin A/C:B1 was significantly reduced, indicating that hMSCs have a similar lamin A/C profile to that seen on soft matrices (Figure 3C). Additionally, we observed that the nuclei of hMSCs on hydrogels with a higher tan(δ) had a smaller area and lower solidity, which indicate reduced nuclear spreading and correlate with a phenotype for reduced lamin A/C expression (Figure S6H–M, Supporting Information).

3.4. Cell–Cell Communication in hMSCs Is Regulated by the Matrices' Viscous Component

Cell–cell communication is crucial for chondrogenesis.[2] Indeed, micromass/pellet cultures are used as scaffold-free chondrogenic systems by facilitating high density cell–cell contacts and mesenchymal condensation.[32] Wnt signaling, involving *N*-cadherin and β-catenin, is a crucial event in cell–cell-mediated chondrogenesis, with canonical Wnt activation and β-catenin accumulation having been implicated as negative regulators in this process.[33] Repressed Wnt/β-catenin signaling is likely to be involved in early chondrogenesis, as inhibition for 3 days was reported to increase chondrogenic gene expression.[20] Here, we observed that, on PAAm gels with a higher tan(δ), hMSCs cultured for 3 days expressed higher levels of *N*-cadherin, which was localized to the cell–cell junctions within clusters of aggregated cells; minimal clustering and lower *N*-cadherin levels were instead observed on gels with a lower tan(δ) (**Figure 4**A). We also observed an increase in *N*-cadherin expression by qPCR as well as a concomitant downregulation in β-catenin, which is likely to facilitate early chondrogenesis through *N*-cadherin-mediated inhibition of β-catenin (Figure 4B).[19] This increased cell clustering was also seen in a 3D PEG-MAL environment with a higher tan(δ) (Figure 4C) and coincided with increased *N*-cadherin expression and reduced β-catenin (Figure 4D). It is likely that increased clustering due to viscoelastic mechanoregulation of hMSCs facilitates *N*-cadherin mediated inhibition of β-catenin.

3.5. hMSC Chondrogenesis Is Facilitated in Matrices with a Higher Loss Tangent

Following the observations that the adhesive, mechanotransductive, and cell–cell interactive behavior of hMSCs in environments with a higher tan(δ) was representative of a chondrogenic phenotype, we next characterized their early and late chondrogenic differentiation in basal conditions. SOX9 is arguably the master regulator of chondrogenesis; its high expression is crucial for the maintenance of the chondrocyte phenotype[34] and regulates the expression of cartilage matrix markers collagen II and aggrecan through direct binding and regulation of their promotor elements.[35] Here, we observed an increase in SOX9 expression for hMSCs in environments with a higher tan(δ) both in 2D and in 3D (**Figure 5**Ai,Bi and Figure S9A, Supporting Information), and a concomitant downregulation in early osteogenic marker Runx2 expression (Figure S9B, Supporting Information). Runx2 is a master regulator of osteogenesis and one of the main antagonists of SOX9; there is a clear interdependent relationship between both proteins, as high Runx2 levels depress SOX9 expression,[36] while elevated SOX9 inhibits Runx2.[37] Interestingly, we also observed an increased expression of Piezo1 for hMSCs in environments with a stronger viscous character (Figure S10, Supporting Information); Piezo1, a mechanosensitive, stress-activated Ca^{2+} ion channel[38] recently shown to interact directly with cadherins,[39] has been implicated as a marker of chondrogenesis, as it is robustly expressed in articular chondrocytes.[40]

To further characterize the differentiation of hMSCs, we investigated the expression of cartilage matrix markers COL2A1 and aggrecan after prolonged culture times. We observed elevated expression of both markers in environments with higher tan(δ); this was accompanied by a downregulation in markers of chondrocyte hypertrophy COL10A1 and fibrocartilage COL1A1 compared to gels with a lower tan(δ) (Figure 5Aii-v,Bii-v and Figure S9C,D, Supporting Information).[41,42] Furthermore, the use of chondrogenic induction medium during culture enhanced the expression of cartilage matrix deposition only in more elastic environments, while it had no effect in higher tan(δ) hydrogels, suggesting that their mechanical properties alone saturated the cell response (Figure 5B and Figure S9C,D, Supporting Informa-

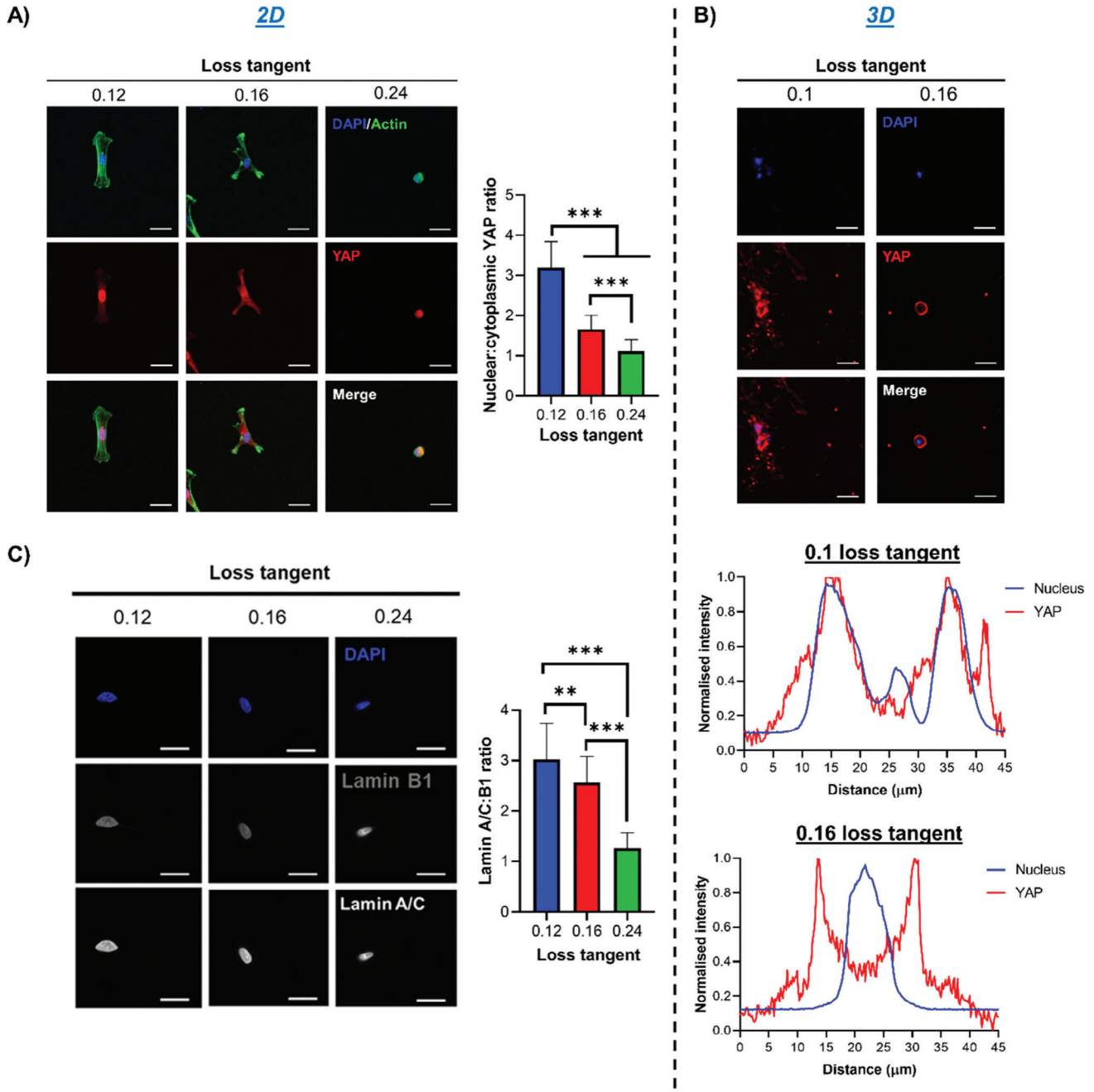

Figure 3. hMSC mechanotransduction is regulated by the matrix viscous component. A) hMSCs cultured for 3 days on 2D PAAm gels before staining for DAPI (blue), actin (green), and YAP (red), with representative immunofluorescence images (left) and quantification of nuclear:cytoplasmic YAP ratio (right), $n = 22–30$. B) hMSCs cultured for 3 days in 3D PEG-MAL gels before staining for DAPI (blue) and YAP (red), with representative immunofluorescence images (top) and representative line scan analysis of nuclear and YAP intensity using "plot profile" in ImageJ (bottom), showing that YAP is mainly nuclear in more elastic gels and cytoplasmatic in more viscous ones. C) Representative immunofluorescence images of hMSCs cultured for 3 days on 2D PAAm hydrogels with DAPI (blue), lamin B1 and A/C staining (left), and quantification of lamin A/C:B1 ratio (right), $n = 30–31$. For all figures, data are represented as mean ± standard deviation and differences are considered significant for $p \leq 0.05$ using one-way ANOVAs for multiple comparisons (** $p \leq 0.01$, *** $p \leq 0.001$). All hydrogels were functionalized with 2 mM RGD peptide to allow cell adhesion. All PEG-MAL hydrogels were crosslinked using peptide ratios of 1% VPM and 99% scrambled VPM. Scale bars = 20 μm.

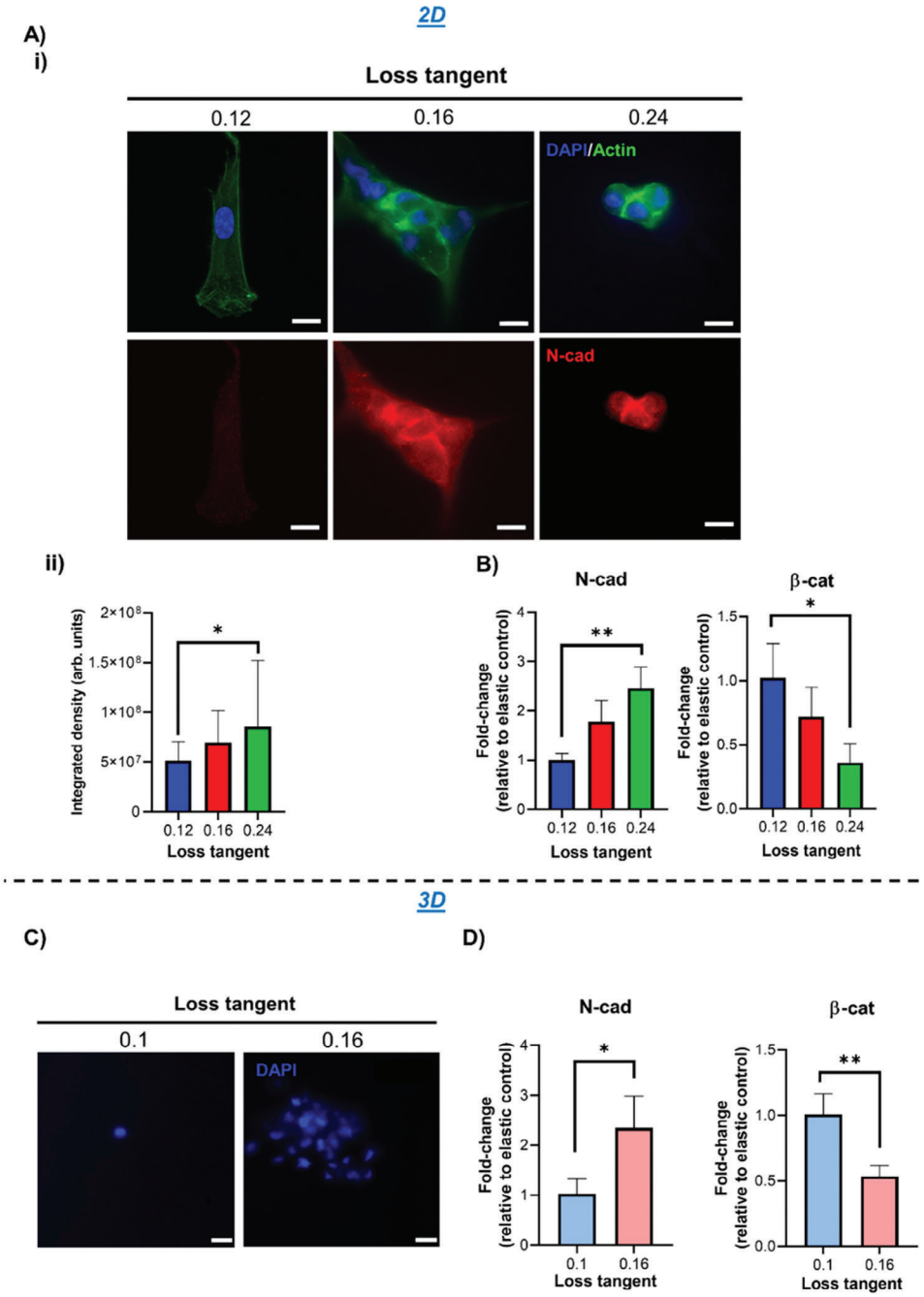

Figure 4. hMSC cell–cell signaling is enhanced in matrices with a higher loss tangent. A-i) Representative immunofluorescence images of hMSCs cultured for 3 days on 2D PAAm hydrogels with DAPI (blue), actin (green), and *N*-cadherin (red) staining, and ii) quantification of *N*-cadherin expression by integrated density, $n = 26$. B) qPCR data from hMSCs cultured on 2D PAAm hydrogels for 3 days showing fold-change in gene expression of *N*-cadherin (left) and *β*-catenin (right) relative to control with stronger elastic character (0.12 loss tangent samples) and normalized to GAPDH, $n = 3$. C) Representative images of DAPI-stained hMSCs after 3 days of culture in 3D PEG-MAL hydrogels. D) qPCR data from hMSCs cultured in 3D PEG-MAL hydrogels for 3 days showing fold-change in gene expression of *N*-cadherin (left) and *β*-catenin (right) relative to the control with stronger elastic character (0.1 loss tangent samples) and normalized to GAPDH, $n = 3$. For all figures, data are represented as mean ± standard deviation, and differences are considered significant for $p \leq 0.05$ using one-way ANOVAs and *t*-test for multiple and pairwise comparisons respectively (* $p \leq 0.05$, ** $p \leq 0.01$). Integrated density quantification was normalized to cell number based on the number of nuclei in each image. All hydrogels were functionalized with 2 mM RGD peptide to allow cell adhesion. All PEG-MAL hydrogels were crosslinked using peptide ratios of 1% VPM and 99% scrambled VPM. Scale bars = 20 μm.

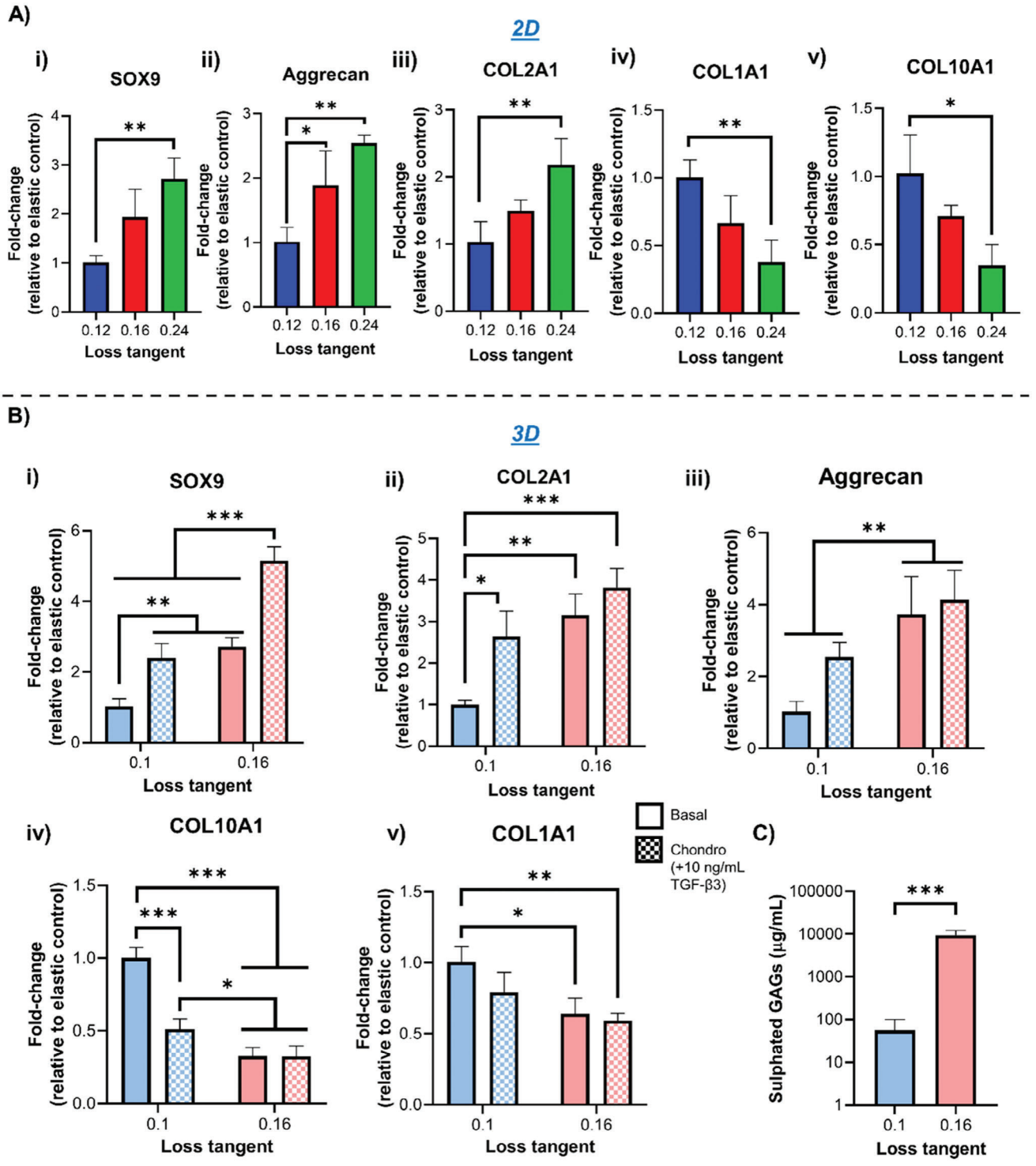

Figure 5. hMSC chondogenesis is promoted in matrices with a higher loss tangent. A) qPCR data showing fold-change in gene expression from hMSCs following i) 3-day culture on 2D PAAm hydrogels for SOX9 and ii) 7 days for Aggrecan, iii) COL2A1, iv) COL1A1, and v) COL10A1, $n = 3$. B) qPCR data showing fold-change in gene expression from hMSCs cultured in 3D PEG-MAL hydrogels for i) 3 days for SOX9 and ii) 7 days for Aggrecan, iii) COL2A1, iv) COL1A1, and v) COL10A1, $n = 3$. Cells were cultured in either basal medium or chondrogenic medium containing 10 ng mL^{-1} TGF-β3. C) Sulfated GAG quantification from hMSCs following 3-week cultures in 3D PEG-MAL hydrogels, $n = 3$. For all figures, data are represented as mean ± standard deviation, and differences are considered significant for $p \leq 0.05$ using one-way ANOVA and *t*-tests for multiple and pairwise comparisons respectively (* $p \leq 0.05$, ** $p \leq 0.01$, *** $p \leq 0.001$). All hydrogels were functionalized with 2 mM RGD peptide to allow cell adhesion. All qPCR data was made relative to control sample with stronger elastic character (0.12/0.1 loss tangent) and normalized to GAPDH. All PEG-MAL hydrogels were crosslinked using peptide ratios of 1% VPM and 99% scrambled VPM.

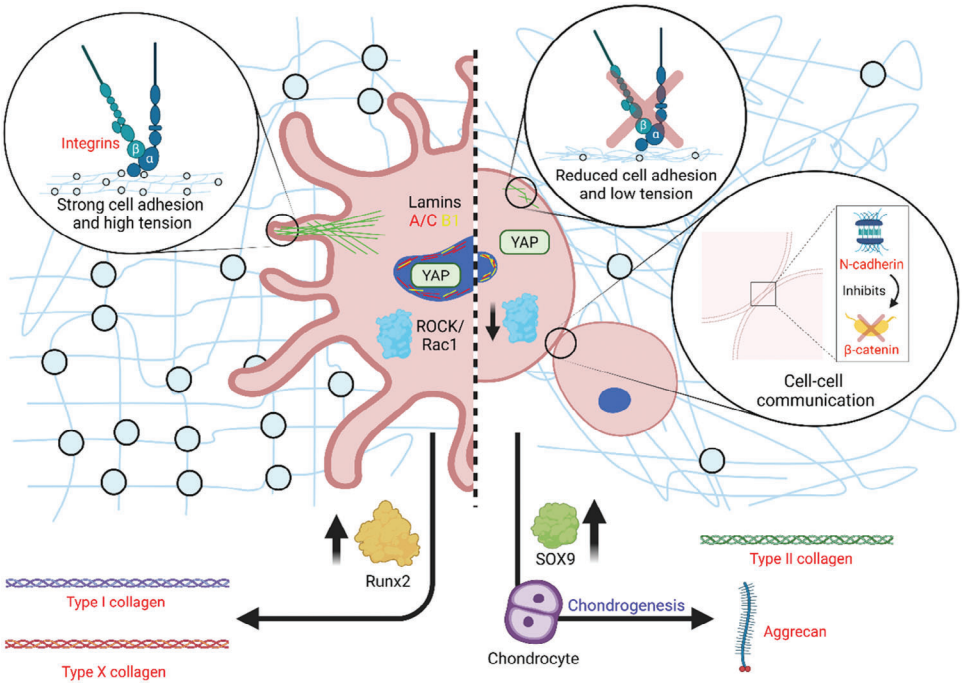

Figure 6. Mechanoregulation of hMSC differentiation in microenvironments with fixed elasticity and varied loss tangent. Using 12 kPa hydrogels, in an environment with a stronger elastic character hMSCs take on a highly spread, tensile phenotype with high expression of integrins and focal adhesions that apply high traction forces. This behavior facilitates mechanotransduction and expression of genes and proteins implicated in fibrocartilage and chondrocyte hypertrophy. In an environment with a higher viscous component, hMSCs take on a small, rounded phenotype with low cytoskeletal tension (comparable to a ROCK/Rac1-inhibited phenotype) and reduced integrin expression that diminishes cell traction forces to the ECM. This response inhibits mechanotransduction and promotes cell–cell contact through cell clustering, with increased *N*-cadherin expression and inhibition of *β*-catenin activity. Collectively, these responses drive chondrogenesis through increased expression of SOX9 and secretion of cartilage matrix markers. Figure generated using BioRender online software.

tion). Matrix secretion was further characterized via staining of aggrecan and COL2A1 in PEG-MAL gels, showing elevated levels of secreted cartilage matrix in hydrogels with a higher tan(δ) compared to those with a lower one (Figures S11 and S12, Supporting Information). Sulfated glycosaminoglycans (GAGs) content was also quantified; we observed a significant increase in their amount from cells cultured in more viscous hydrogels compared to more elastic ones (Figure 5C).

Overall, the higher loss tangent of the isoelastic hydrogels developed in this study influenced the adhesive, mechanotransductive, and cell–cell behavior of hMSCs to favor commitment to a chondrogenic lineage. Importantly, the downregulation of chondrocyte hypertrophy and fibrocartilage markers suggests neocartilage formation, as also evidenced by the matrix markers staining in 3D environments (Figures S11 and S12, Supporting Information). Finally, it is important to highlight that the observed hMSC behavior occurs independently of gel degradability. Indeed, when the amount of degradable crosslinker VPM was increased from 1 to 100%, similar responses were observed, in terms of adhesion, early signaling, and matrix markers expression (Figure S13, Supporting Information).

4. Discussion

Most studies investigating the role of stem cell mechanosensitivity in chondrogenesis focus solely on the elasticity of the cells' environment, with Young's modulus of the substrates ranging from ≈10 to ≈1000 kPa.[2] The viscous nature of the materials is generally disregarded. This has led to contradictory results, which could partly be attributed to interference from unreported variability in viscous modulus.[2] While some studies have suggested that the viscous character of the substrates may be important during stem cell chondrogenesis, its contribution to the materials employed in these works is accompanied by a change in the elastic modulus or by the confounding effect of other biochemical cues.[6–8] Therefore, the role of the materials' viscous component in these biological processes remains elusive. Our work provides a comprehensive study of hMSC response to a variation of the viscous properties of 2D and 3D culture environments, eliminating any potential influence of the elastic character of the substrate. Using isoelastic matrices in growth factor-free conditions, we have explored a variety of cell responses to changes in substrate viscosity, including adhesion and spreading behavior, mechanotransduction, cell–cell signaling, and differentiation.

Our results obtained on isoelastic matrices with Young's moduli of ≈12 kPa indicate that matrices exhibiting a more viscous character (high tan(δ)) promote a chondrogenic hMSC phenotype, facilitated by a rounded cell shape with reduced adhesion and low cytoskeletal tension (**Figure 6**). Instead, more elastic matrices (lower tan(δ)) support increased cell spreading and cytoskeletal tension, with high expression of integrins and focal

adhesions that apply high traction forces; this promotes the expression of genes and proteins implicated in fibrocartilage and chondrocyte hypertrophy (Figure 6). The reduced cell spreading observed in more viscous environments coincides with a decrease in nuclear mechanotransduction of YAP and in lamin A/C levels; YAP, which is considered a mechanical rheostat, was previously less understood in the context of hydrogel-driven stem cell chondrogenesis.[29] Here, we show that the mechanically-driven downregulation of YAP nuclear translocation correlates with a chondrogenic response of hMSCs. Viscous matrices also lead to a downregulation of ROCK and Rac1 signaling, with ROCK being known to negatively regulate chondrogenesis.[30,43–45] Moreover, the matrix viscous component affects cell–cell contacts, with a high expression of *N*-cadherin and a downregulation of *β*-catenin in more viscous environments; such repression of Wnt signaling has been previously shown to stimulate early chondrogenesis.[19,20,46] Collectively, these cellular responses facilitate stem cell chondrogenesis through increased expression of SOX9, COL2A1 and aggrecan in the more viscous matrices compared to the more elastic ones, as evidenced through qPCR at an earlier stage (7 days) and immunofluorescence at a later stage (3 weeks); biochemical analysis of sulfated GAGs also confirmed increase in this chondrogenic marker at a late timepoint (Figure 5). We believe that the more viscous hydrogels that we have engineered mechanically facilitate a low tension rounded/clustered MSC phenotype, typically promoted by higher seeding densities in hydrogel-free cultures; this phenotype is known to be highly chondroinductive, driving changes in chondrogenic gene markers from early timepoints.[47,48] In particular, significant changes in chondrogenic gene expression, for example, COL2A1 and aggrecan, have been observed at 3/7 days timepoints when MSCs are cultured in hydrogels that support chondrogenesis.[49,50]

Importantly, here we also demonstrate that the observed effects are independent of the material platform used and of its dimensionality. Similar viscoelastic properties of matrices with different compositions prompt similar responses, either when cells are seeded on 2D PAAm, or when they are encapsulated within 3D PEG-MAL matrices. In the latter case, we critically show that the intrinsic viscous character of the matrix is the dominant factor in determining cell response rather than degradability, as higher VPM content does not alter the increased chondroinductive potential of viscous environments compared to their more elastic counterparts (Figure S13, Supporting Information).

In conclusion, we have shown that the cells' mechanotransductive response to the viscous nature of their environment is key to determine the stem cell chondrogenic fate. Controlling the matrices' viscous nature alone provides a growth factor-free, purely mechanically regulated way of efficiently targeting chondrogenesis of hMSCs and promoting the formation of neocartilage. The viscous and elastic components of hydrogels can therefore be better utilized as valuable parameters during the engineering of cartilage (or indeed other tissues), to harness the mechanosensitive response of stem cells and direct their fate toward specific lineages.

Supporting Information

Supporting Information is available from the Wiley Online Library or from the author.

Acknowledgements

This work was funded by a grant from the UK Regenerative Medicine Platform. M.C. and D.G., respectively, acknowledge MRC funding (MR/S005412/1) and Royal Society of the United Kingdom funding under the Wolfson award (RSWF/FT/191020).

Conflict of Interest

The authors declare no conflict of interest.

Data Availability Statement

The data that support the findings of this study are openly available in Enlighten Research Data at http://doi.org/10.5525/gla.researchdata.1545.

Keywords

chondrogenesis, hydrogels, mechanotransduction, stem cells, viscoelasticity

Received: October 6, 2023
Revised: November 14, 2023
Published online: December 12, 2023

[1] M. Asadishekari, E. N. Mpoyi, Y. Li, J. Eslami, M. Walker, M. Cantini, D. Gourdon, *Front. Phys.* **2022**, *10*, 806554.
[2] M. Walker, J. Luo, E. W. Pringle, M. Cantini, *Mater. Sci. Eng., C* **2021**, *121*, 111822.
[3] O. Chaudhuri, J. Cooper-White, P. A. Janmey, D. J. Mooney, V. B. Shenoy, *Nature* **2020**, *584*, 535.
[4] M. Cantini, H. Donnelly, M. J. Dalby, M. Salmeron-Sanchez, *Adv. Healthcare Mater.* **2020**, *9*, e1901259.
[5] O. Chaudhuri, *Biomater. Sci.* **2017**, *5*, 1480.
[6] W. Li, D. Wu, D. Hu, S. Zhu, C. Pan, Y. Jiao, L. Li, B. Luo, C. Zhou, L. Lu, *Mater. Sci. Eng., C* **2020**, *107*, 110333.
[7] D. Huang, Y. Li, Z. Ma, H. Lin, X. Zhu, Y. Xiao, X. Zhang, *Sci. Adv.* **2023**, *9*, eade9497.
[8] H. J. Lee, Y. Seo, H. S. Kim, J. W. Lee, K. Y. Lee, *ACS Omega* **2020**, *5*, 15567.
[9] Z. Gong, S. E. Szczesny, S. R. Caliari, E. E. Charrier, O. Chaudhuri, X. Cao, Y. Lin, R. L. Mauck, P. A. Janmey, J. A. Burdick, V. B. Shenoy, *Proc. Natl. Acad. Sci. USA* **2018**, *115*, E2686.
[10] O. Chaudhuri, L. Gu, M. Darnell, D. Klumpers, S. A. Bencherif, J. C. Weaver, N. Huebsch, D. J. Mooney, *Nat. Commun.* **2015**, *6*, 6364.
[11] E. Hui, K. I. Gimeno, G. Guan, S. R. Caliari, *Biomacromolecules* **2019**, *20*, 4126.
[12] H.-P. Lee, L. Gu, D. J. Mooney, M. E. Levenston, O. Chaudhuri, *Nat. Mater.* **2017**, *16*, 1243.
[13] M. Brittberg, A. Lindahl, A. Nilsson, C. Ohlsson, O. Isaksson, L. Peterson, *N. Engl. J. Med.* **1994**, *331*, 889.
[14] S. Roberts, J. Menage, L. J. Sandell, E. H. Evans, J. B. Richardson, *Knee* **2009**, *16*, 398.
[15] H. Le, W. Xu, X. Zhuang, F. Chang, Y. Wang, J. Ding, *J. Tissue Eng.* **2020**, *11*, 204173142094383.
[16] N. W. Marion, J. J. Mao, *Methods Enzymol.* **2006**, *420*, 339.
[17] J. T. Connelly, A. J. García, M. E. Levenston, *J. Cell. Physiol.* **2008**, *217*, 145.
[18] A. Woods, G. Wang, F. Beier, *J. Cell. Physiol.* **2007**, *213*, 1.
[19] E. Haÿ, E. Laplantine, V. Geoffroy, M. Frain, T. Kohler, R. Müller, P. J. Marie, *Mol. Cell. Biol.* **2009**, *29*, 953.

[20] R. Li, J. Xu, D. S. H. Wong, J. Li, P. Zhao, L. Bian, *Biomaterials* **2017**, *145*, 33.
[21] J. R. Tse, A. J. Engler, *Curr. Protoc. Cell Biol.* **2010**, *10*, 6.
[22] E. E. Charrier, K. Pogoda, R. G. Wells, P. A. Janmey, *Nat. Commun.* **2018**, *9*, 449.
[23] A. R. Cameron, J. E. Frith, J. J. Cooper-White, *Biomaterials* **2011**, *32*, 5979.
[24] A. J. García, *Ann. Biomed. Eng.* **2014**, *42*, 312.
[25] L. E. Jansen, L. J. Negrón-Piñeiro, S. Galarza, S. R. Peyton, *Acta Biomater.* **2018**, *70*, 120.
[26] O. Chaudhuri, L. Gu, D. Klumpers, M. Darnell, S. A. Bencherif, J. C. Weaver, N. Huebsch, H.-P. Lee, E. Lippens, G. N. Duda, D. J. Mooney, *Nat. Mater.* **2016**, *15*, 326.
[27] B. D. Cosgrove, K. L. Mui, T. P. Driscoll, S. R. Caliari, K. D. Mehta, R. K. Assoian, J. A. Burdick, R. L. Mauck, *Nat. Mater.* **2016**, *15*, 1297.
[28] A. Karystinou, A. J. Roelofs, A. Neve, F. P. Cantatore, H. Wackerhage, C. De Bari, *Arthritis Res. Ther.* **2015**, *17*, 147.
[29] C. Yang, M. W. Tibbitt, L. Basta, K. S. Anseth, *Nat. Mater.* **2014**, *13*, 645.
[30] A. Woods, G. Wang, F. Beier, *J. Biol. Chem.* **2005**, *280*, 11626.
[31] A. Buxboim, J. Swift, J. Irianto, K. R. Spinler, P. C. D. P. Dingal, A. Athirasala, Y.-R. C. Kao, S. Cho, T. Harada, J.-W. Shin, D. E. Discher, *Curr. Biol.* **2014**, *24*, 1909.
[32] A. L. Carlberg, B. Pucci, R. Rallapalli, R. S. Tuan, D. J. Hall, *Differentiation* **2001**, *67*, 128.
[33] M. I. Reinhold, R. M. Kapadia, Z. Liao, M. C. Naski, *J. Biol. Chem.* **2006**, *281*, 1381.
[34] Q. Zhao, H. Eberspaecher, V. Lefebvre, B. De Crombrugghe, *Dev. Dyn.* **1997**, *209*, 377.
[35] H. Akiyama, *Mod. Rheumatol.* **2008**, *18*, 213.
[36] A. Cheng, P. G. Genever, *J. Bone Miner. Res.* **2010**, *25*, 2680.
[37] J. Liao, N. Hu, N. Zhou, L. Lin, C. Zhao, S. Yi, T. Fan, W. Bao, X. Liang, H. Chen, W. Xu, C. Chen, Q. Cheng, Y. Zeng, W. Si, Z. Yang, W. Huang, *PLoS One* **2014**, *9*, e89025.
[38] J. L. Nourse, M. M. Pathak, *Semin. Cell Dev. Biol.* **2017**, *71*, 3.
[39] J. Wang, J. Jiang, X. Yang, G. Zhou, L. Wang, B. Xiao, *Cell Rep.* **2022**, *38*, 110342.
[40] W. Gao, H. Hasan, D. E. Anderson, W. Lee, *Front. Cell Dev. Biol.* **2022**, *10*, 885224.
[41] R. M. Salasznyk, W. A. Williams, A. Boskey, A. Batorsky, G. E. Plopper, *J. Biomed. Biotechnol.* **2004**, *2004*, 24.
[42] G. Shen, *Orthod. Craniofacial Res.* **2005**, *8*, 11.
[43] J. L. Allen, M. E. Cooke, T. Alliston, *Mol. Biol. Cell* **2012**, *23*, 3731.
[44] N. Sahu, G. Budhiraja, A. Subramanian, *Stem Cell Res. Ther.* **2020**, *11*, 6.
[45] D. A. Foyt, D. K. Taheem, S. A. Ferreira, M. D. A. Norman, J. Petzold, G. Jell, A. E. Grigoriadis, E. Gentleman, *Acta Biomater.* **2019**, *89*, 73.
[46] Q. Liu, W. Wang, L. Zhang, L. Zhao, W. Song, X. Duan, Y. Zhang, *Biomaterials* **2014**, *35*, 6206.
[47] Z. Li, B. Cao, X. Wang, K. Ye, S. Li, J. Ding, *J. Mater. Chem. B* **2015**, *3*, 5197.
[48] B. Cao, Y. Peng, X. Liu, J. Ding, *ACS Appl. Mater. Interfaces* **2017**, *9*, 23574.
[49] S. Mahzoon, J. M. Townsend, T. N. Lam, V. Sjoelund, M. S. Detamore, *Ann. Biomed. Eng.* **2019**, *47*, 2308.
[50] L. Bian, M. Guvendiren, R. L. Mauck, J. A. Burdick, *Proc. Natl. Acad. Sci. USA* **2013**, *110*, 10117.
[51] G. Ciccone, M. Azevedo Gonzalez Oliva, N. Antonovaite, I. Lüchtefeld, M. Salmeron-Sanchez, M. Vassalli, *J. Visualized Exp.* **2022**, *179*, e63401.
[52] Y. M. Efremov, T. Okajima, A. Raman, *Soft Matter* **2020**, *16*, 64.
[53] L. Oliver-Cervelló, H. Martin-Gómez, C. Gonzalez-Garcia, M. Salmeron-Sanchez, M.-P. Ginebra, C. Mas-Moruno, *Front. Bioeng. Biotechnol.* **2023**, *11*, 1192436.
[54] A. N. Buxton, J. Zhu, R. Marchant, J. L. West, J. U. Yoo, B. Johnstone, *Tissue Eng.* **2007**, *13*, 2549.
[55] S. Trujillo, C. Gonzalez-Garcia, P. Rico, A. Reid, J. Windmill, M. J. Dalby, M. Salmeron-Sanchez, *Biomaterials* **2020**, *252*, 120104.
[56] P. B. Welzel, S. Prokoph, A. Zieris, M. Grimmer, S. Zschoche, U. Freudenberg, C. Werner, *Polymers* **2011**, *3*, 602.
[57] T. Canal, N. A. Peppas, *J. Biomed. Mater. Res.* **1989**, *23*, 1183.
[58] N. A. Peppas, E. W. Merrill, *J. Polym. Sci., Polym. Chem. Ed.* **1976**, *14*, 441.
[59] G. M. Cruise, D. S. Scharp, J. A. Hubbell, *Biomaterials* **1998**, *19*, 1287.
[60] E. Merrill, K. Dennison, C. Sung, *Biomaterials* **1993**, *14*, 1117.
[61] M. B. Mellott, K. Searcy, M. V. Pishko, *Biomaterials* **2001**, *22*, 929.
[62] N. A. Peppas, E. W. Merrill, *J. Appl. Polym. Sci.* **1977**, *21*, 1763.
[63] U. Horzum, B. Ozdil, D. Pesen-Okvur, *MethodsX* **2014**, *1*, 56.
[64] A. Boudaoud, A. Burian, D. Borowska-Wykret, M. Uyttewaal, R. Wrzalik, D. Kwiatkowska, O. Hamant, *Nat. Protoc.* **2014**, *9*, 457.
[65] Q. Tseng, E. Duchemin-Pelletier, A. Deshiere, M. Balland, H. Guillou, O. Filhol, M. Théry, *Proc. Natl. Acad. Sci. USA* **2012**, *109*, 1506.